

## **PREDICTING STRENGTH OF THERMOPLASTIC POLYMER PARTS PRODUCED USING ADDITIVE MANUFACTURING**

Joseph Bartolai<sup>\*</sup>, Timothy W. Simpson<sup>\*</sup>, and Renxuan Xie<sup>†</sup>

<sup>\*</sup>Department of Mechanical and Nuclear Engineering

<sup>†</sup>Department of Chemical Engineering

The Pennsylvania State University, University Park, PA

### **Abstract**

The weakest point in polymer parts produced by Fused Filament Fabrication (FFF) is the interface between adjacent layers and deposition toolpaths, or “roads”. We introduce a novel approach that uses the temperature history of these interfaces, polymer rheological data, and polymer welding theory to predict the mechanical strength of parts subjected to uniaxial tension. Interface temperature history data is collected in-situ using infrared imaging. Rheological data of the polycarbonate (PC) used to fabricate the parts in this study was determined experimentally. The prediction of strength of the interfaces was performed using polymer weld theory from the literature adapted to the PC feedstock used in this study. Understanding how the strength of the road and layer interfaces develop mechanical strength will lead to stronger FFF parts through intelligent toolpath optimization and temperature control.

### **Introduction**

Additive Manufacturing (AM) is the process of creating a prototype or end-use part by adding material in a layer-by-layer process. In Fused Filament Fabrication (FFF), this is accomplished by extruding a thermoplastic material from a nozzle that translates in three dimensions, depositing material first on a heated surface then upon previously deposited material. The FFF process is analogous with Fused Deposition Modeling (FDM). The weakest point of these parts occurs at the boundary between adjacent layers and adjacent deposition toolpaths, or roads.<sup>1,2</sup>

A novel approach for predicting the strength of parts produced by FFF is proposed in this paper to determine the strength of these interfaces using polymer weld theory, polymer rheology, temperature history of the interface, and the forces applied to the interface. To demonstrate this approach, test specimens are subjected to uniaxial tension parallel to the as-built layer planes. Saint-Venant’s principle is applied to the bulk test specimen and it is assumed that all layers are loaded equally, resulting in no forces occurring across the inter-layer interfaces. This analysis considers only the interaction of the interfaces between adjacent deposition roads. All further references to the interface describe this inter-road interface.

Prediction of the strength of the thermoplastic polymer part requires: the thermal history of the interface, the temperature dependent longest reptation relaxation time of the polymer, the area of the weld interface, the loading subjected to the part, and the ultimate tensile strength (UTS) of the polymer in the amorphous bulk. Each piece of information was gathered experimentally, with the exception of the UTS of the bulk polymer where strength data published by the material manufacturer was used. Polycarbonate (PC) was chosen for the experiments because all of the material was known to be from the same production lot and processing history from pellet to filament feedstock to finished part was known to the authors.

AM production of the test specimen was performed on a Sell's Mendel RepRap, which is an FFF AM machine. The machine was equipped with an E3D v5 hot end (E3D-Online, Oxfordshire, UK), RAMBo 1.3L motherboard (UlitMachine, South Pittsburg, TN, USA), and Panucatt Helios 200 heated build platform (Panucatt Devices, Irvine, CA, USA). The RepRap was run on the open-source Marlin 1.1 firmware. Gcode was generated using Slic3r, an open-source slicing and gcode generation software. The machine interface was performed using Printron Prointerface software, which is also open-source. All tensile specimens were produced in the YXZ orientation with infill toolpath orientations alternating  $\pm 45^\circ$  from the Y-axis of the machine. Two perimeter deposition passes were used in the production process. A detailed diagram of the toolpaths used can be found in the Appendix. Tensile testing was performed following the procedure outlined in ASTM D638. Experimental data was collected from ten tensile specimens.<sup>3,1</sup>

### Polymer Weld Theory

When two thermoplastic polymer surfaces are joined by welding, strength is developed by the diffusion of polymer chains across the welding interface. A polymer weld that is kept above a temperature and allows molecular motion for a sufficient amount of time can have strength equal to that of the polymer bulk. This is illustrated in Figure 1, originally published by Grewell and Benatar.<sup>6</sup> In the case of parts produced by FFF, these welds will not be held at

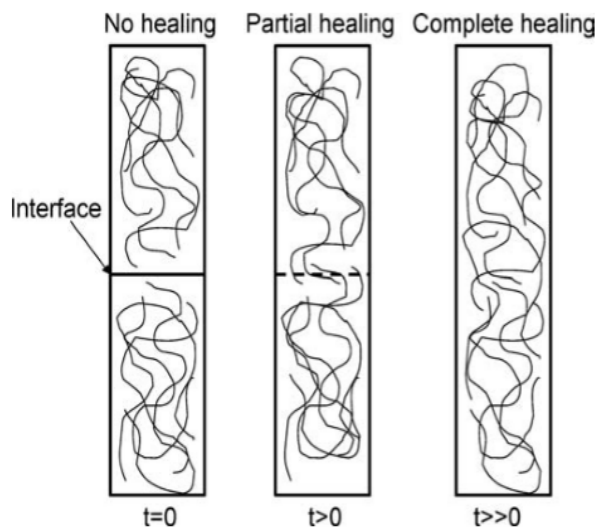


Figure 1: Molecular healing of a polymer-polymer weld interface over time, from Grewell and Benatar.<sup>6</sup>

boundaries, strength is developed. The thermal history of these interfaces determines the weld strength, as the polymer chains are more free to move within the bulk. Weld strength increases as the amount of time the interface is exposed to temperatures sufficient to allow molecular diffusion within the polymer bulk to the one-quarter power. More simply stated, the weld strength increases with  $t_{weld}^{1/4}$ .<sup>7</sup>

Strength predictions were carried out using the relationship in Equation 1, which is adapted from Ezekoye et al.:<sup>4</sup>

sufficient temperature to become fully healed; so, the microstructure will resemble the partially healed case shown in Figure 1. Consider the case where one end of a polymer chain remains in that chain's parent bulk, but the other end migrates across the interface through diffusion and becomes entangled with polymer chains on the other side of the interface. If a load is applied across the boundary, it would be transferred from one bulk to the other by this chain and all others that have one end on each side of the interface. The corresponding weld has two possible failure modes: (1) chain pullout and (2) chain fracture.<sup>4-6</sup>

In FFF, the weld interface is the interface between adjacent roads and adjacent layers. As polymer chains cross these

$$\frac{\sigma_{weld}}{\sigma_{UTS}} = \left( \frac{t_{weld}}{\bar{\tau}_{rep}} \right)^{1/4} \quad (1)$$

In Equation 1,  $\sigma_{weld}$  is the weld strength (in MPa),  $\sigma_{UTS}$  is the ultimate tensile strength (in MPa),  $t_{weld}$  is the time of molecular activity at the interface (in seconds), and  $\bar{\tau}_{rep}$  is the time average reptation time of the polymer (in seconds). As  $t_{weld}$  approaches  $\bar{\tau}_{rep}$ , the weld interface becomes fully healed. Ezekoye et al.<sup>4</sup> expanded the relationship to replace the reptation relaxation time with a diffusion constant and the radius of gyration of the polymer. A calculated time average polymer interdiffusion constant was then used to predict the weld strength. These terms are omitted here, as change of reptation relaxation time with temperature is used to make the strength prediction.<sup>4</sup>

### **Polymer Rheology**

The temperature dependent longest reptation relaxation time of the PC used in these experiments was determined experimentally using parallel plate shear rheometry. The sample was conformed to a disk shape with diameter of 8 mm and thickness of 1.2 mm via vacuum assisted molding at 285 °C. Rheometry experiments were performed using a Rheometric Scientific ARES-LS (TA Instruments, New Castle, DE, USA) rheometer in a Nitrogen (N<sub>2</sub>) environment. The dynamic shear modulus  $G^* = G' + iG''$ , where  $G'$  is shear storage modulus and  $G''$  is shear loss modulus, was measured in the frequency range from 0.4 rad/s to 100 rad/s with a controlled strain of 0.5%. The isothermal frequency sweep experiment was conducted from 300 °C to 150 °C with a step of -20 °C. The reptation relaxation time has been shown to be equal to the reciprocal of the low frequency crossing point of  $G'$  and  $G''$ .<sup>8</sup> This crossing point was found to be 10 rad/s at 200 °C, as shown in Figure 2, which gives a reptation relaxation time of 0.1 s at 200 °C.

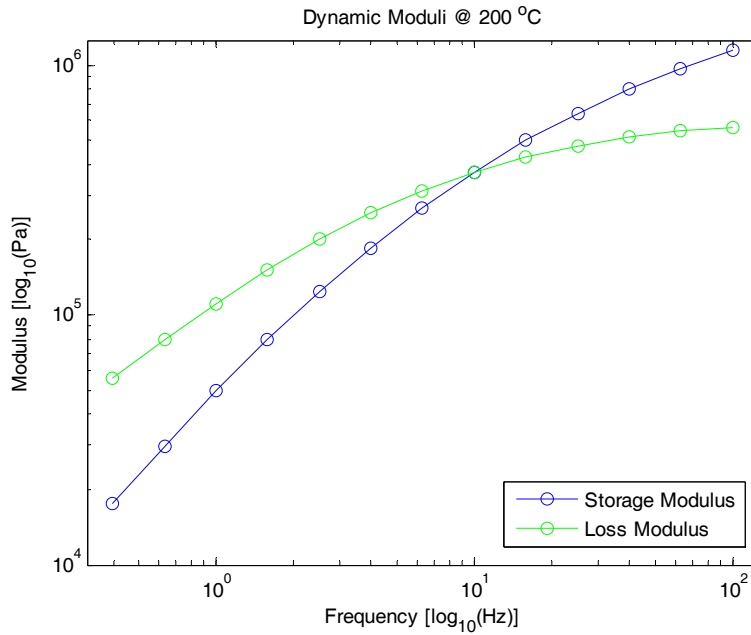


Figure 2: Experimental PC shear storage and loss moduli vs. frequency at 200 °C.

Time-Temperature Superposition (TTS) was used to determine shift factors ( $a_T$ ) for each temperature relative to 200 °C. TTS master curves for storage and loss modulus of the PC used in this study can be found in the Appendix. The TTS shift factors were used to find the constants of the Williams-Landel-Ferry (WLF) equation<sup>9</sup>, which was then used to calculate the shift factor for a given temperature. The shift factors produced by the WLF equation were then applied to determine the reptation relaxation time at a given temperature. The WLF equation is given in Equation 2, and the temperature dependence of  $\tau_{rep}$  is given in Equation 3.

$$\log(a_T) = \frac{-C_1(T-T_{ref})}{C_2+(T-T_{ref})} \quad (2)$$

$$\tau_{rep}(T) = \tau_{rep}(T_{ref}) \times a_T \quad (3)$$

Equations 2 and 3 can then be combined to provide an expression for the temperature-dependent reptation relaxation time:

$$\tau_{rep}(T) = \tau_{rep}(T_{ref}) \times \exp\left(\frac{-C_1(T-T_{ref})}{C_2+(T-T_{ref})}\right) \quad (4)$$

The constants for the WLF equation were found to be  $C_1 = 4.29$  and  $C_2 = 87.7$ . These constants were determined by a least squares best fit using the MATLAB Curve Fitting Tool (MathWorks, Natick, MA, USA). It should be noted that these constants are only valid for this particular PC using 200 °C as the reference temperature. A comparison between the curve generated using these constants and the experimental time shift factors is shown in Figure 3.

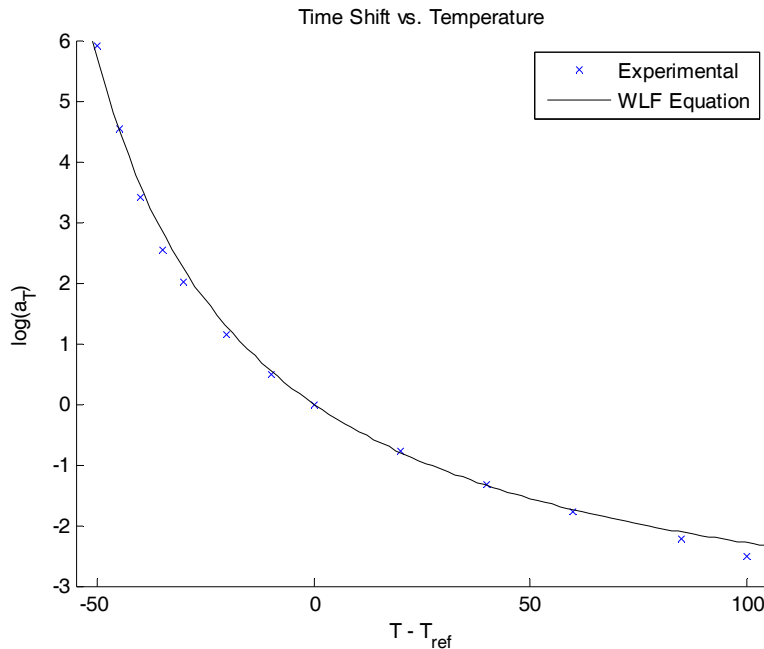


Figure 3: Experimental and WLF Equation Calculated time shift vs. Temperature, where  $T_{ref}$  is 200 °C.

### Measurement of Weld Interface Temperature History

Obtaining the thermal history of the weld interface is crucial for determining the strength of that interface. Temperature history of the weld interface was measured by infrared (IR) imaging using an Optris Pi 400 IR camera and Optris Pi Connect process monitoring software (Optris GmbH, Berlin, DE). An E3D PT-100 thermocouple (E3D-Online, Oxfordshire, UK) was used as a reference temperature measurement. In-situ temperature measurements were performed during AM builds of the tensile specimens on the Sells Mendel RepRap. Test specimens were built using identical temperatures, feed rates, and toolpath distances, but at different build orientations to facilitate ease of temperature measurement. The temperature measurement at these different build orientations is equal and uniform across the build plate due to the open-air build volume of the Sells Mendel. An IR image of the in-situ measurement is shown in Figure 4 and the equivalent measurement is shown in Figure 5. The temperatures measured in the experiments shown in Figures 4 and 5 were assumed to be equivalent, as the tool path length, tool speed, deposition rate, deposition temperature, and ambient temperatures were all equal. Temperatures measured during the experiment in Figure 5 were used to calculate strength because build location allowed for an increase in pixel resolution of the area of interest and eliminated any measurement error due to reflection of heat from the nozzle assembly.

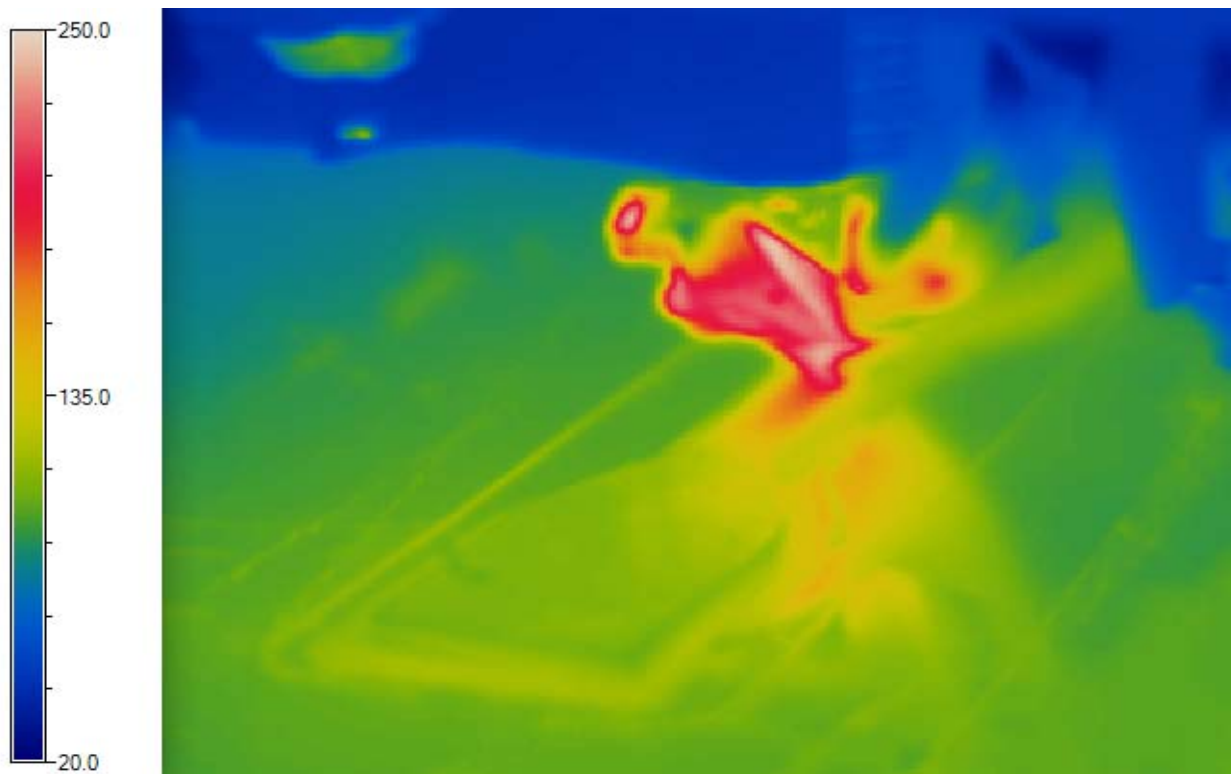


Figure 4: In-situ temperature measurement of PC tensile specimen build process. Reference temperatures are shown in degrees Celsius.

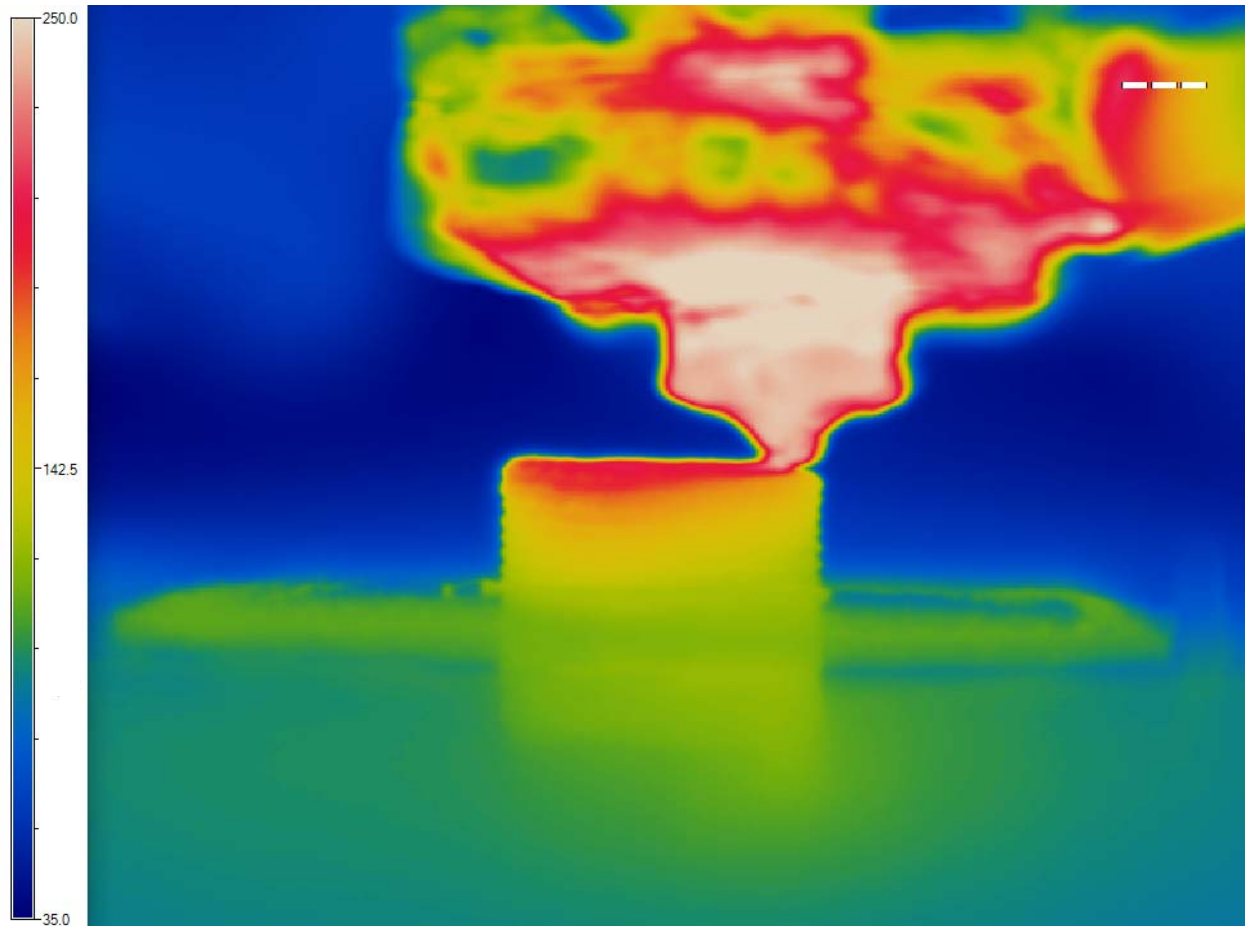


Figure 5: Temperature measurement in the alternate orientation experiment. Reference temperatures shown are in Celsius.

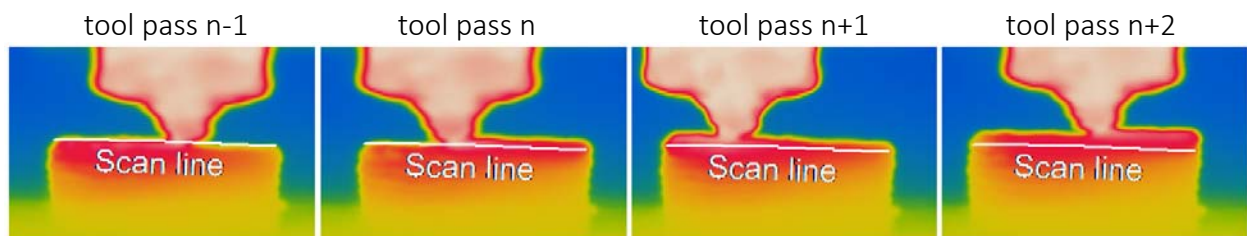


Figure 6: IR image of temperature measurement experiment with tool passes  $n-1$  through  $n+2$  shown. Scan line denotes the line from which temperature data is output by Optris Pi Connect software.

Figure 6 details how the weld interface temperature measurements were collected. IR images from four tool passes are shown in the figure. The “scan line” from the Optris Pi Connect software denotes the line at which temperature measurement occurred. A temperature value was recorded for each pixel on the line once per frame. Measurement framerate was 10 Hz. Figure 7 shows a weld interface thermal history including two tool passes before material is deposited in the area of interest. The interface thermal history shown in Figure 8 was used in the weld strength calculations. Temperature was measured at the centerline of the gage region, as this location exhibited a temperature history least desirable for developing weld strength.

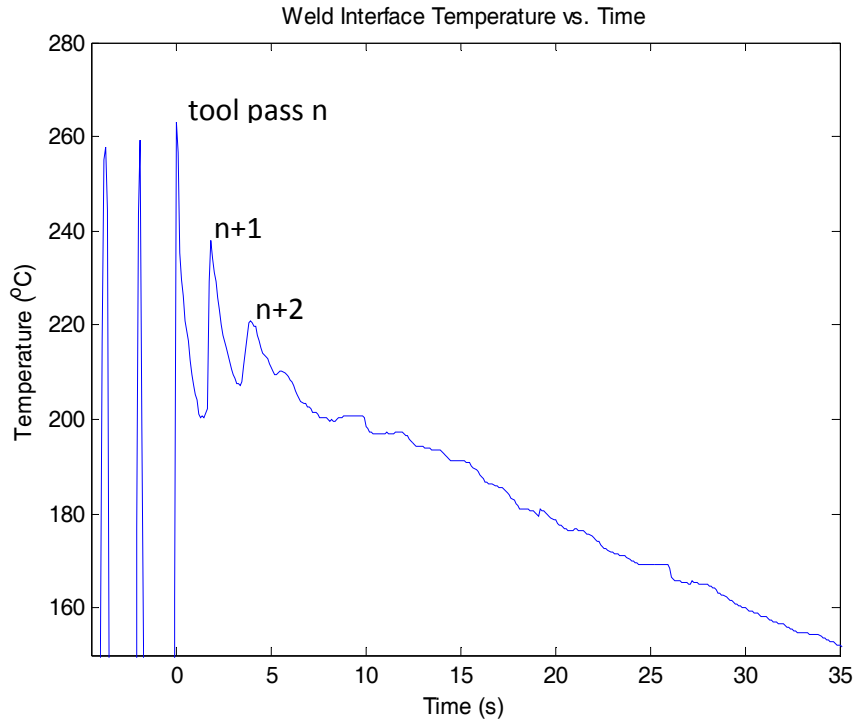


Figure 7: Temperature history of weld interface including two tool passes before the deposition of material. Tool pass where material is first deposited at the weld interface is denoted as tool pass  $n$ . Subsequent tool passes are denoted  $n+1$  and  $n+2$ .

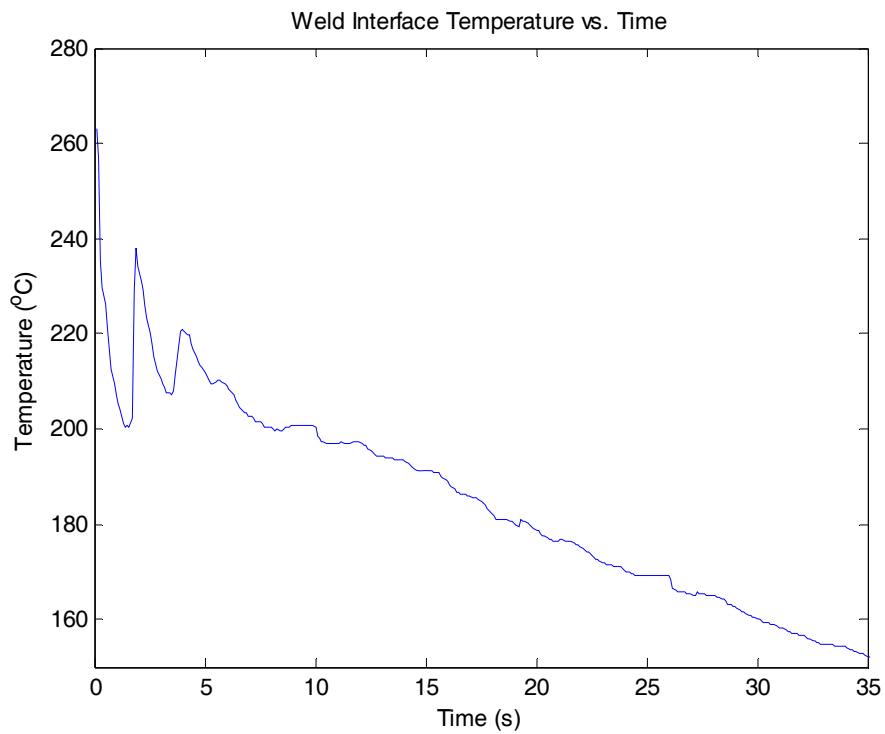


Figure 8: Weld interface temperature history used in weld strength calculations.

## Calculating Predicted Tensile Strength

To determine the predicted tensile strength of the produced part, the rule of mixtures was used to combine the weld strength with the strength of the perimeter roads that lie parallel to the gage axis. The void space, where the rounded edges of the deposited cross-section fail to fill the rectangular voxel, is also considered using this model. Figure 9 illustrates this phenomena, which is also observable in Figure 10. This is accomplished by assigning a tensile strength of zero to the void space. For the perimeter tool passes, the entire area of the deposited material was considered to contribute a strength equal to that of the bulk material UTS with a cross-sectional area equal to what was measured for a single road cross-section. The weld strength at the inter-road interfaces was considered to contribute a strength equal to the calculated weld strength with a cross sectional area equal to the weld interface length in the gage region of the tensile specimen multiplied by the smallest road interface length, measured parallel to the specimen Z-axis. The smallest measured length was used as this location would be weakest. These areas were determined using optical microscope images of specimen fracture surfaces. One such image is shown in Figure 10.

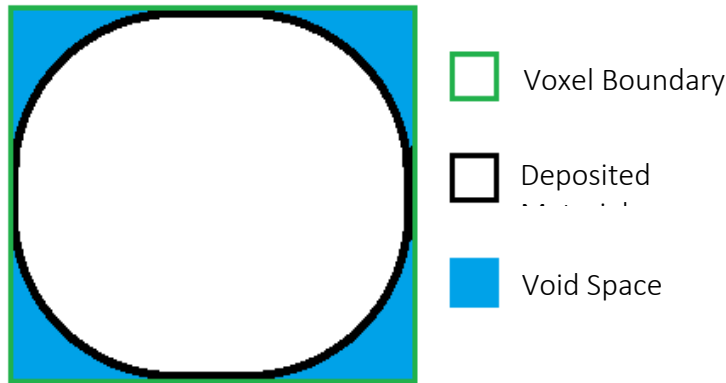


Figure 9: Illustration of deposited material partially filling the desired voxel.

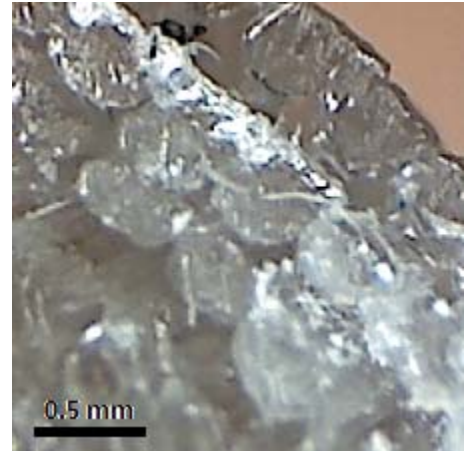


Figure 10: Cross-sectional view of tensile specimen.

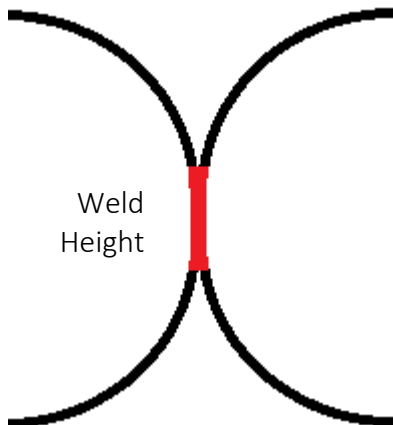


Figure 11: Illustration of weld height. Length measured for the weld height is shown in red.



Figure 12: Illustration of gage region toolpaths. Perimeter roads are shown in red; infill roads are shown in blue.

The cross section of one layer in the gage region, equal to the layer height multiplied by the gage width, was calculated to be 1.75 mm<sup>2</sup>. Cross-sectional areas of the perimeter roads and the weld interfaces were then calculated. The cross-section of the perimeter roads in one layer was measured to be 0.40 mm<sup>2</sup>. Weld interface area was calculated by measuring the weld interface height and multiplying by the toolpath interface length. The minimum weld interface area in one layer was calculated to be 0.65 mm<sup>2</sup>. The minimum weld height at the fracture surface was used to determine this weld interface area, as the weld interface with the smallest area at the fracture surface was assumed to be the initial point of failure. An illustration of how weld height was measured can be found in Figure 11. Figure 12 shows a subset of the tensile specimen gage region tool paths. Perimeter roads are shown in red; infill roads are in blue.

It should be noted that weld area was calculated parallel to the toolpath direction, not perpendicular to the gage length. Consider a polymer chain crossing the weld interface, with each end entangled in the polymer bulk on either side of the interface. If a force was applied to one polymer bulk in a direction perpendicular to the weld interface and the other was rigidly constrained, then the load would be transferred between the two polymer bulks by the polymer chain traversing the weld interface. The weld would fail when one end of the polymer chain pulls out of its entanglements or the chain itself fractures.<sup>4-6</sup> Now consider the case where the load is applied parallel to the weld interface. Again, failure would occur by either chain pullout or chain fracture. Both cases can be accounted for if the polymer chain that joins the interfaces is considered to be a two-force member loaded in tension. With this consideration, loading of the weld interface in any direction will have equal strength to welds loaded perpendicular to the weld interface, as studied by Ezekoye et al.<sup>4</sup>

This assumption led to the area fractions of  $f_{per} = 0.23$  and  $f_{weld} = 0.37$ . These were used with the rule of mixtures to calculate a UTS for the AM produced part, as shown in Equation 5:

$$\sigma_{AM} \leq \left( \frac{f_{per}}{\sigma_{UTS}} + \frac{f_{weld}}{\sigma_{weld}} \right)^{-1} \quad (5)$$

where  $\sigma_{weld}$  is determined from Equation 1, rearranged as shown in Equation 6. Using the temperature history shown in Figure 8 and Equation 4, then averaging over the weld time,  $\bar{t}_{rep}$  was found to be 1.75s. This was much shorter than  $t_w$ , which was 32.5s. Therefore, the weld was determined to be fully healed with a strength equal to the bulk UTS. Using Equation 5 and the material manufacturer's reported bulk UTS of 65 MPa, the predicted strength of the part was found to be  $\sigma_{AM} = 39 \text{ MPa}$ . This is compared with experimental results in Table 1, which is based on ten samples.

$$\sigma_{weld} = \left( \frac{t_{weld}}{\bar{t}_{rep}} \right)^{1/4} \times \sigma_{UTS} \quad (6)$$

Table 1: Comparison of predicted and experimental strength of PC test specimens.

Predicted Strength	Experimental Strength
39 MPa	35.4 ± 2.93 MPa

## Conclusion and Directions for Future Work

While the predicted strength of the tensile specimen was slightly greater than the upper bound of the 95% confidence window of the experimental strength, the theory presented herein shows promise for better understanding of how strength is developed in thermoplastic polymer parts manufactured using an AM process, specifically Fused Filament Fabrication (FFF). Future work will include expanding testing to additional polymers and different specimen geometry. Because the combination of a short tool path return time and even shorter  $\bar{\tau}_{rep}$ , polymer weld theory played a somewhat small part in the strength calculation. Future experiments will be performed on polymers with a longer relaxation time to study this in more detail. The PC used in this experiment had a relatively low viscosity for use in FFF. A polymer of higher viscosity would have longer relaxation times. ASTM D638 Type I specimen will also be considered for future experiments, as the greater gage width will allow for longer tool path times.

## References

1. ISO/ASTM. *ISO/ASTM 52900-2015: Additive manufacturing -- General principles -- Terminology. ISO/ASTM Standards* (2015).
2. Gibson, I., Rosen, D. W. & Stucker, B. *Additive Manufacturing Technologies: Rapid Prototyping to Direct Digital Manufacturing*, Springer, New York, 2010.
3. ASTM. ASTM: D638, Standard test method for tensile properties of plastics. *ASTM Stand.* 1–16 (2013). doi:10.1520/D0638-10.1
4. Ezekoye, O. A, Lowman, C. D., Fahey, M. T. & Hulme-Lowe, A. G. Polymer weld strength predictions using a thermal and polymer chain diffusion analysis. *Polym. Eng. Sci.* **38**, 976–991 (1998).
5. Wool, R. P., Yuan, B. L. & McGarel, O. J. Welding of polymer interfaces. *Polym. Eng. Sci.* **29**, 1340–1367 (1989).
6. Grewell, D. & Benatar, A. Welding of plastics: Fundamentals and new developments. *International Polymer Processing* **22**, 43–60 (2007).
7. Jud, K., Kausch, H. H. & Williams, J. G. Fracture mechanics studies of crack healing and welding of polymers. *J. Mater. Sci.* **16**, 204–210 (1981).
8. Doi, M. & Edwards, S. F. Dynamics Of Concentrated Polymer Systems Part 1. *J. Chem. Soc., Faraday Trans. II* **74**, 1789–1801 (1978).
9. Williams, M. L., Landel, R. F. & Ferry, J. D. The Temperature Dependence of Relaxation Mechanisms in Amorphous Polymers and Other Glass-forming Liquids<sup>1</sup>. *J. Am. Chem. Soc.* **77**, 3701–3707 (1955).

## Appendix

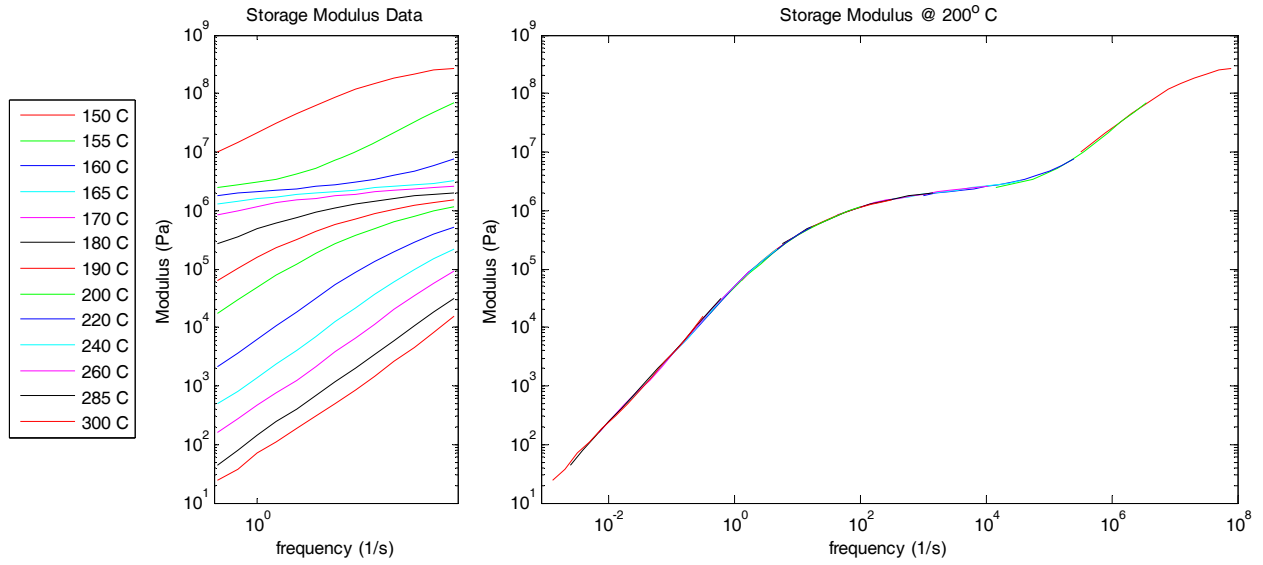


Figure A-1: Experimental and Time-Temperature Superpositioned Shear Storage Modulus vs. Frequency at 200°C.

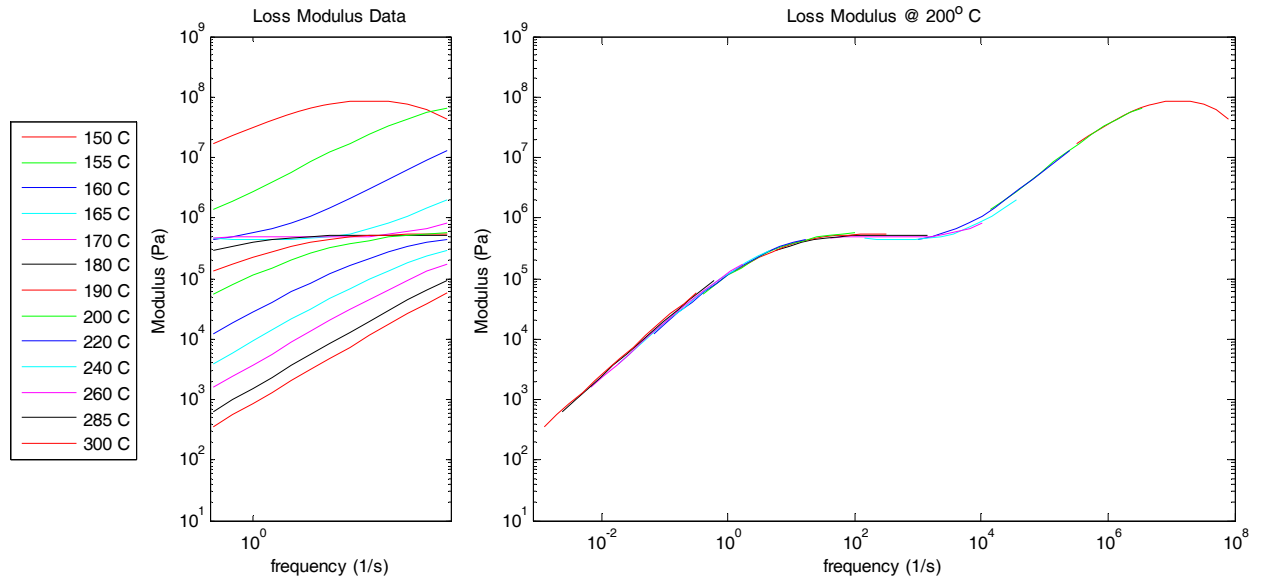


Figure A-2: Experimental and Time-Temperature Superpositioned Shear Loss Modulus vs. Frequency at 200°C.

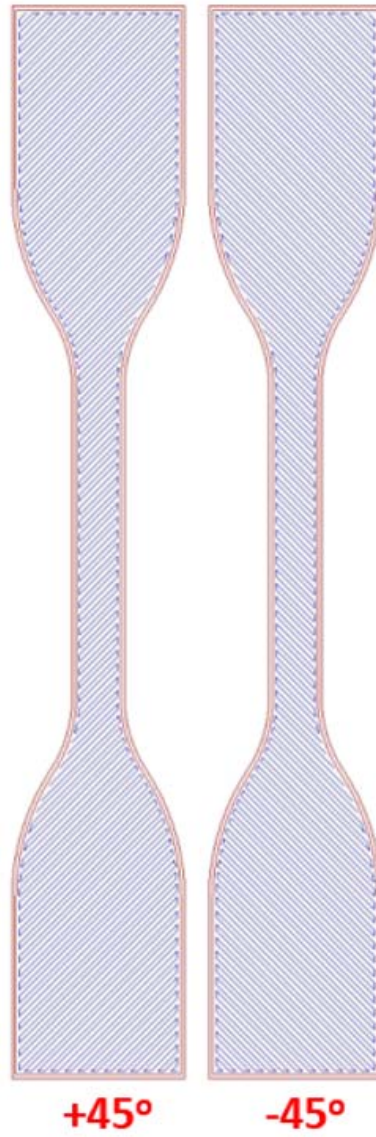


Figure A-3: Illustration of toolpaths used to produce tensile specimens. Infill angles are measured from the machine Y-axis.

## Nomenclature

$\sigma_{AM}$	Additive Manufactured Strength
$\sigma_{UTS}$	Ultimate Tensile Strength
$\sigma_{weld}$	Polymer Weld Strength
$\bar{t}_{rep}$	Time Average Reptation Relaxation Time
AM	Additive Manufacturing
°C	degrees Celsius
CA, USA	California, United States of America
DE	Germany
DE, USA	Delaware, United States of America
FFF	Fused Filament Fabrication
$G^*$	Dynamic Shear Modulus
$G'$	Storage Modulus
$G''$	Loss Modulus
$f_{per}$	Perimeter Area fraction
$f_{weld}$	Weld Interface Area fraction
MA, USA	Massachusetts, United States of America
MPa	10 <sup>6</sup> Pascals
N <sub>2</sub>	Nitrogen
PC	Polycarbonate
TN, USA	Tennessee, United States of America
$t_{weld}$	Weld Exposure Time
TTS	Time-Temperature Superposition
UK	United Kingdom
UTS	Ultimate Tensile Strength